Available online at www.sciencedirect.com
ScienceDirect
Engineering Failure Analysis 14 (2007) 1166–1174
ENGINEERING FAILURE ANALYSIS
www.elsevier.com/locate/engfailanal

Failure analysis of rolls with grooves

Ž. Domazet [a,*], F. Lukša [b], M. Šušnjar [c]

[a] University of Split, Faculty of Electrical Engineering, Mechanical Engineering and Naval Architecture, Ruđera Boškovića bb, 21000 Split, Croatia
[b] Steelworks Split d.d., Industry for Production and Processing Steel, Dr.F.Tuđmana b.b., 21212 Kaštel Sućurac, Croatia
[c] Bit-Art Informatika d.o.o., Pape Ivana Pavla II 31, 21000 Split, Croatia

Received 30 July 2006; accepted 29 November 2006
Available online 27 February 2007

Abstract

The failure analysis of rolls with grooves on a 3-high-roughing mill stand for hot rolling is presented. A detailed analysis of all the elements which influenced failure was carried out, namely, the cause of all failures was determined and all fracture surfaces are described; the rolling forces were determined by analytical and experimental methods; numerical analysis of the local stresses due to rolling forces was performed with the finite element method; stress time history of the individual local stress and stress spectrum were obtained from service loads; properties of the roll material (strength, hardness, toughness and ductility) were determined by experimental testing. Based on the results of investigation, the main causes of the failures are presented.

Keywords: Failure analysis; Roll failures; Hot rolling; Fatigue

1. Introduction

In 'Steelworks Split' failures of the rolls with grooves on the first stand of the 3-high-roughing mill stand (Fig. 1) occurred four times. The 3-high-roughing mill stand was suitable for the hot rolling of the billets with an initial cross-section of 100 mm^2 and 3 m initial length in eight passes. The mass of one billet was 230 kg.

The total length of the roll was 2300 mm, roll barrel length was 1400 mm and roll barrel diameter was 450 mm. The rotation speed of the rolls was 120 rpm. The material used for the rolls was spheroidal graphite iron with a pearlitic base. The hardness on the roll surface was 380 HB. The rolling material was BSt 400 S according to DIN 488. The rolling temperature of the rolling material in the first pass was 1200 °C. The pass schedule and corresponding dimensions are given in Table 1. Fig. 2 shows the roll design and groove distributions with positions of the failures.

* Corresponding author. Tel.: +385 21 305 803; fax: +385 21 463 877.
E-mail address: zeljko.domazet@fesb.hr (Ž. Domazet).

1350-6307/$ - see front matter © 2006 Elsevier Ltd. All rights reserved.
doi:10.1016/j.engfailanal.2006.11.067

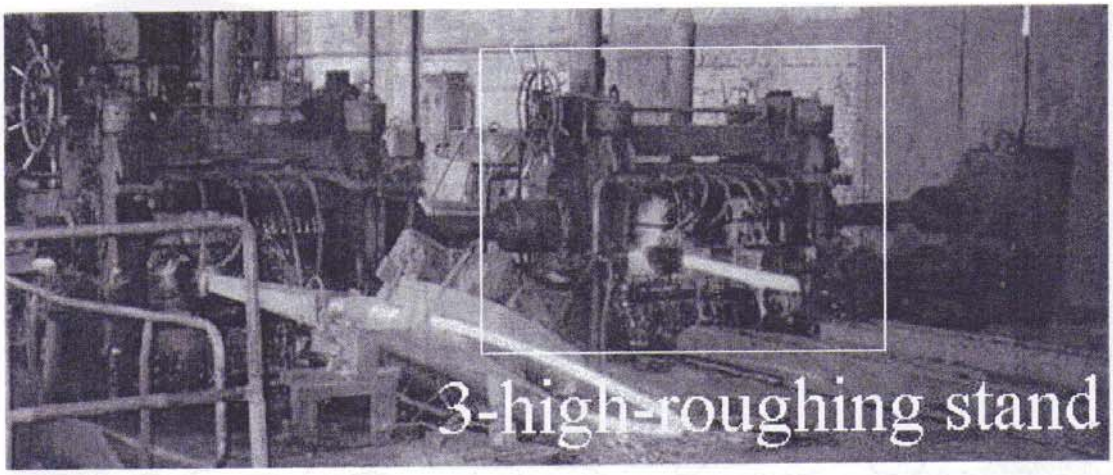

Fig. 1. 3-high-roughing stand.

Table 1
Pass schedule

Pass no.		1	2	3	4	5	6	7	8
Pass shape		Box	Box	Box	Box	Box	Oval	Square	Oval
Groove dimensions (mm)		100 × 82	100 × 66	67 × 80	67 × 59	66 × 52	80 × 34	40	58 × 20
Cross-section (mm^2)	9850	8015	6474	5398	4032	3280	2286	1578	1075
Width (mm)	100	104	108	71	76	65	82.5	53.5	60.5
Initial height (mm)		100.0	82.0	108.0	80.0	76.0	52.0	82.5	40.0
Height after pass (mm)		82.0	66.0	80.0	59.0	52.0	34.0	51.0	20.5
Absolute draught (mm)		18.0	16.0	28.0	21.0	24.0	18.0	31.5	19.5
Absolute reduction (mm^2)		1835	1541	1076	1366	752	994	708	503
Coefficient of elongation		1.23	1.24	1.20	1.34	1.23	1.43	1.45	1.47
Working diameter (mm)		372.5	393.5	372.5	398.5	396.5	419.5	397.25	433
length (m)	3	3.69	4.56	5.47	7.33	9.01	12.93	18.73	27.49
Projected length of arc of contact (mm)		57.84	56.10	72.08	64.68	68.97	61.44	79.10	64.97
Projected area of contact (mm^2)		5900	5947	4938	4754	4276	4531	3461	3265
Rolling time (s)		1.58	1.74	2.26	2.65	3.53	4.65	6.92	9.52
Gap (s)		3	3	3	3	3	3	3	3
Rolling temperature (°C)	1200	1198	1194	1188	1183	1176	1169	1159	1146

2. Fractures of the rolls

The first roll (middle roll) broke after 13 h of operation. Fig. 3 shows the position of the first fracture.

Fig. 4 shows the fracture surfaces of the first broken roll with the position of the stocks at the time of the fracture.

The second roll (middle roll) was dressed after 4000 rolling tons and broke after 10 h of operation after dressing. Fig. 5 shows the fracture surfaces of the second broken roll with the position of the stocks at the time of the fracture.

The third roll (lower roll) was dressed two times, after 4000 rolling tons and then after 8000 rolling tons. This roll broke after the short time of operation after the second dressing. Fig. 6 shows the third broken roll and the fracture surface with the position of the stocks at the time of the fracture.

The fourth roll (upper roll) was dressed after 4500 rolling tons and broke after 568 rolling tons after dressing. Fig. 7 shows the fourth broken roll and the fracture surface with the position of the stocks at the time of the fracture.

A visual examination of the fracture surfaces of the first, second and fourth broken rolls revealed three fracture regions as shown in Figs. 4, 5 and 7: the crack origin zone on the periphery, the crack propagation zone and the final fracture zone. The fracture surfaces of the second and fourth broken rolls were flat while the

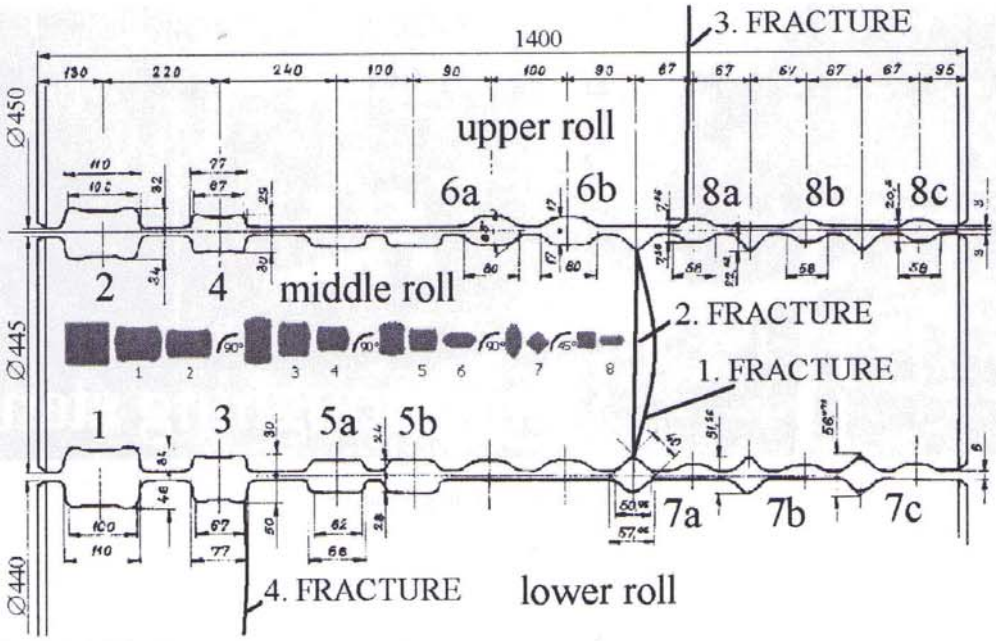

Fig. 2. Roll design and groove distributions.

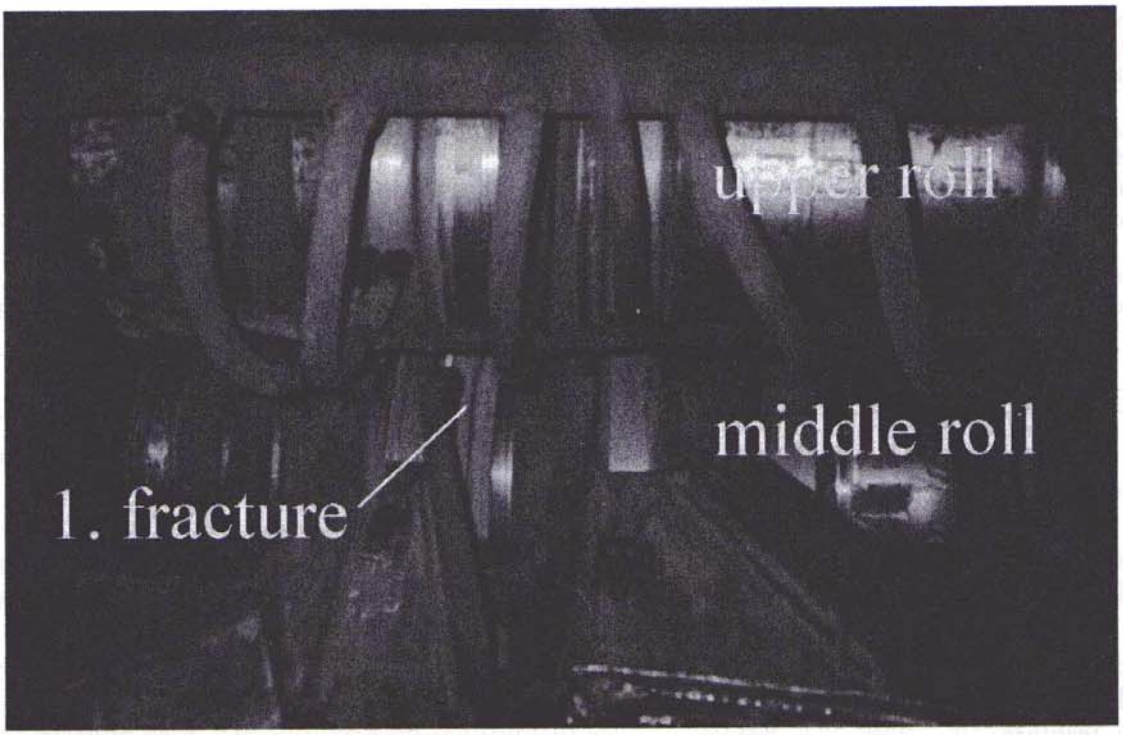

Fig. 3. Position of first fracture (back side of the stand).

fracture surface of the first broken roll was curved. No surface irregularities and no firecracks were present on the fracture surfaces and around the fracture surfaces on the surface of the grooves. The appearance of the fracture surfaces suggested a low-cycle fatigue resulting from rotational-bending loading with a high stress concentration.

A visual examination of the fracture surface of the third broken roll revealed only one fracture region with rough striations from the surface to the centre of the roll. The appearance of the fracture surface of this roll suggested that the fracture had occurred rapidly due to overload by dynamic impact.

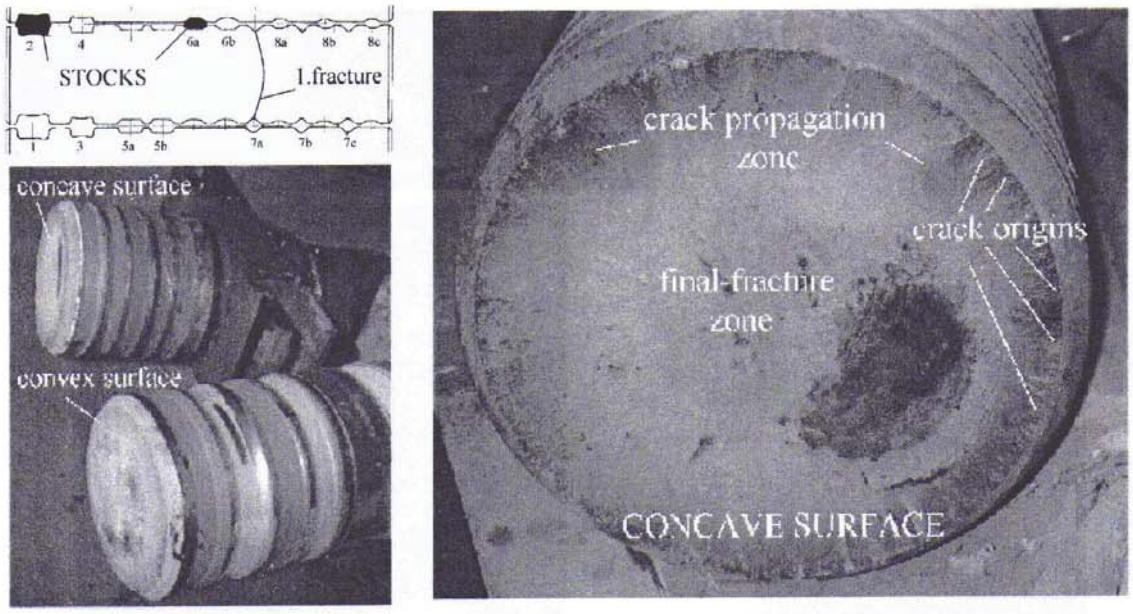

Fig. 4. Fracture surfaces of the 1st broken roll and the position of the stocks in time of the fracture.

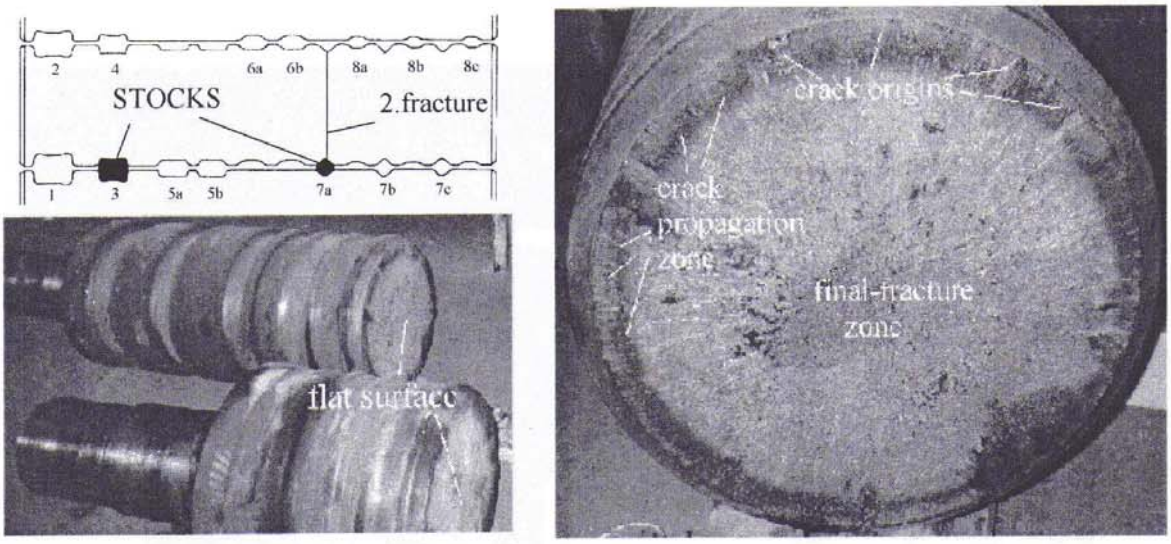

Fig. 5. Fracture surfaces of the 2nd broken roll and the position of the stocks in time of the fracture.

3. Rolling forces

There are several methods used nowadays to calculate the rolling force (A.I. Tselikov, S. Ekelund, A.A. Koroljev, A. Geleji, A.F. Golovin and V.A. Tiagunov, R.B. Sims and E. Siebel), and the results from all are different. Because of numerous parameters (the properties of the rolls and the rolling material, the form of the grooves, the friction between rolls and rolling material, ...) the experimental methods are more suitable for determining the rolling force in grooves.

In accordance with results from analytical methods for determining the rolling force, four measuring devices, with three strain gauges on each, were designed for experimentally determining the rolling force. The measuring devices were mounted on both sides of the stand, instead of safety parts against the breakage of rolls (Fig. 8).

Fig. 9 shows experimental and analytical results of the rolling forces.

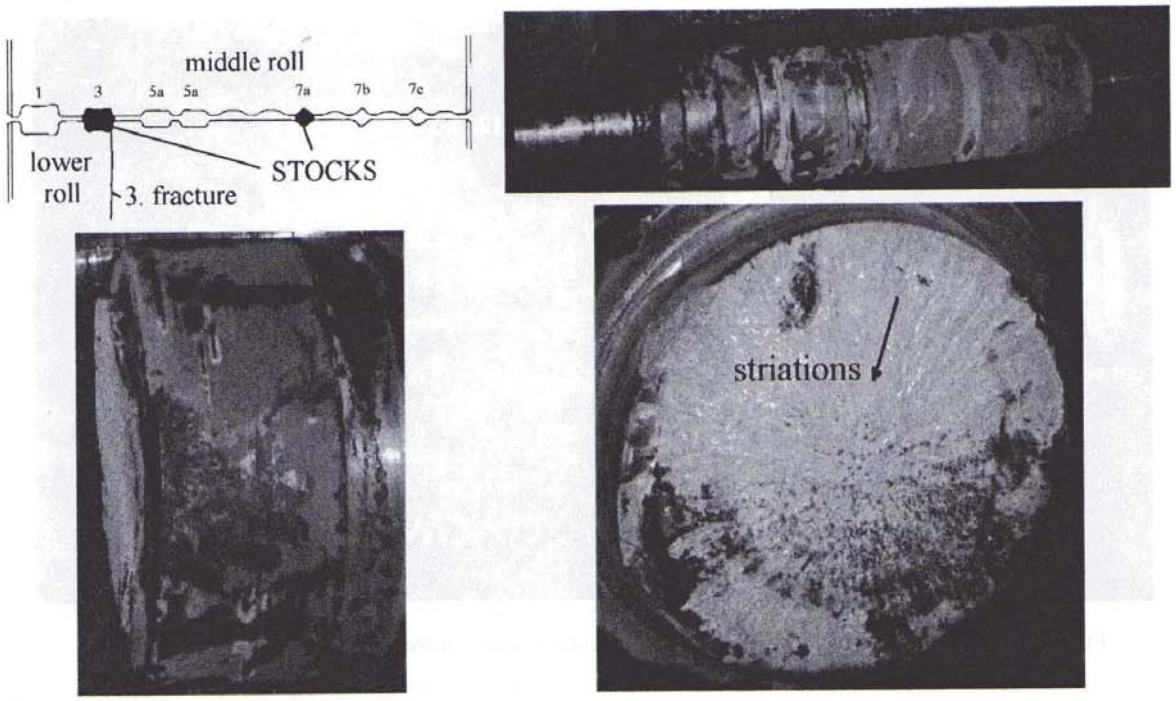

Fig. 6. Fracture surfaces of the third broken roll and the position of the stocks in time of the fracture.

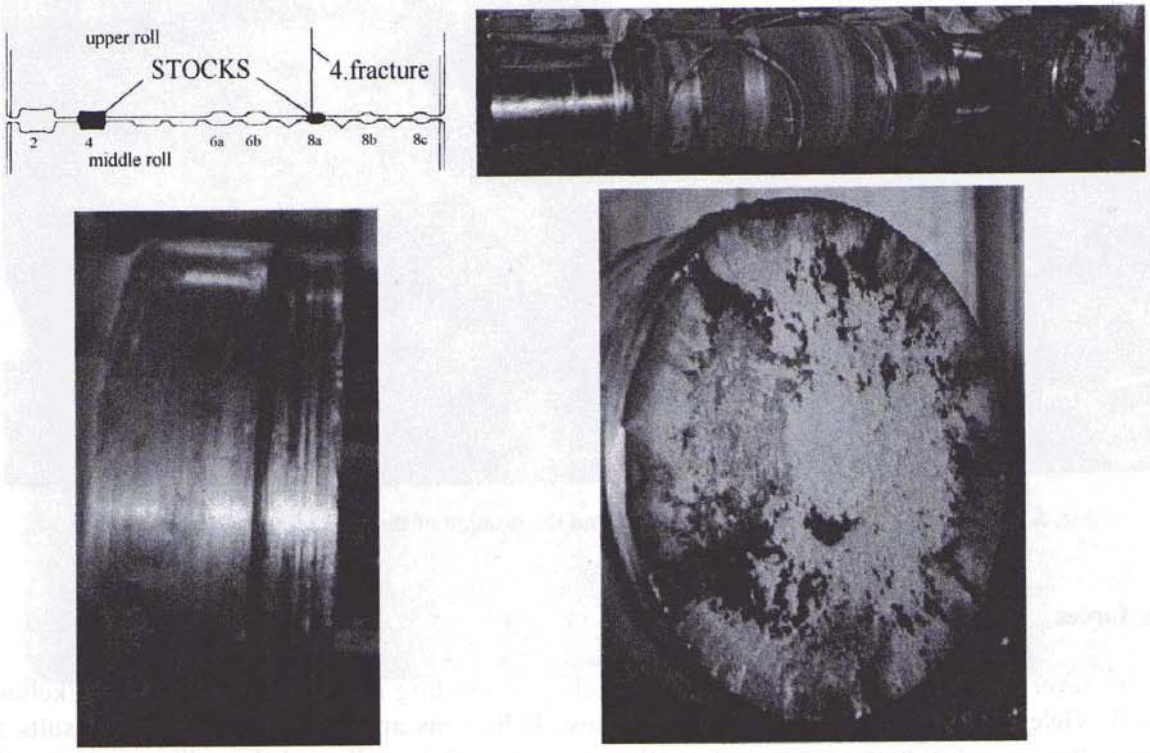

Fig. 7. Fracture surfaces of the fourth broken roll and the position of the stocks in time of the fracture.

4. Stress–time history

The obtained experimental results of the rolling forces are used for numerical analysis of the local stresses by the finite element method. The FEM revealed that the most critical area of the roll is the 7.a pass. A linear elastic model with 3D solid elements with eight DOF per nodes was used. The complete numerical analysis

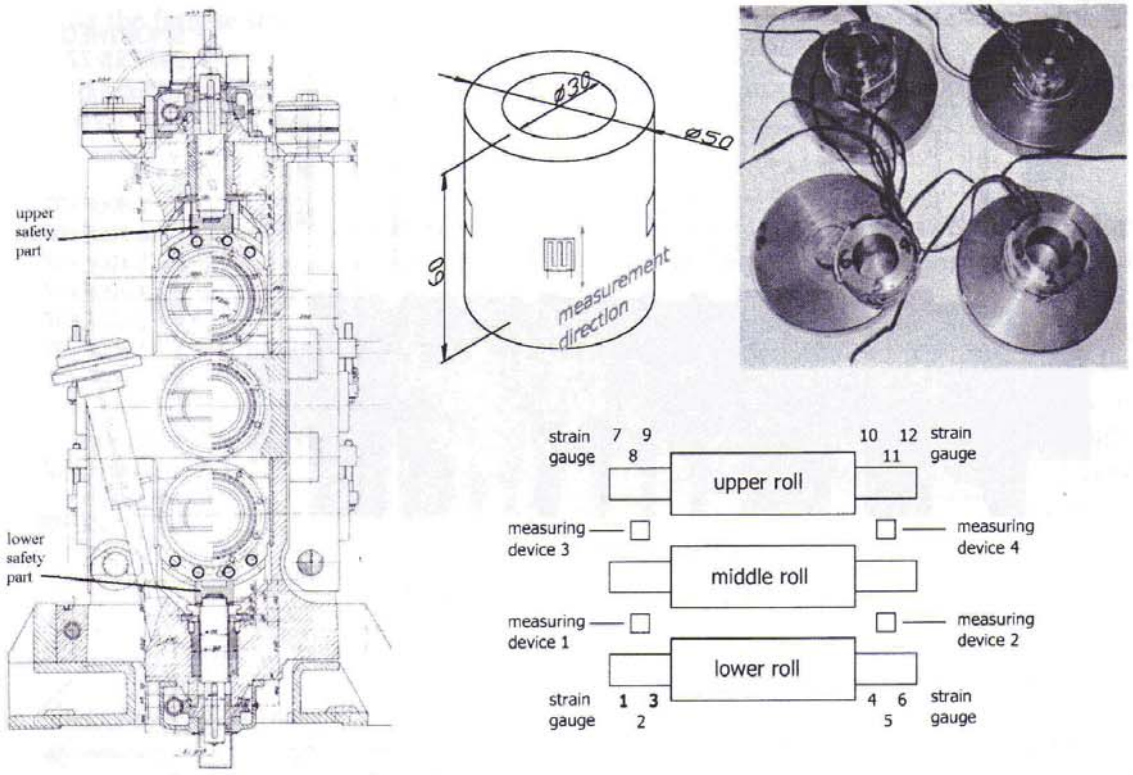

Fig. 8. Measurement system and measuring devices.

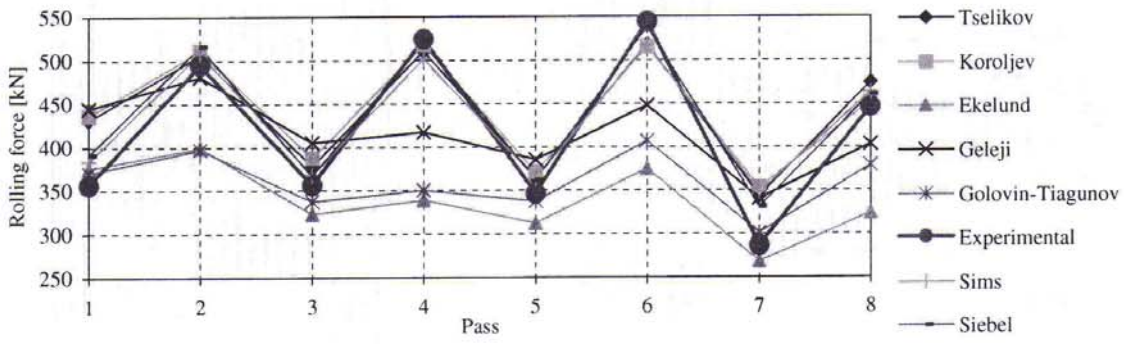

Fig. 9. Analytical and experimental results.

included 30 cases according to the rolling schedule. Fig. 10 shows the FEM model of the middle roll with positions of the stocks in fourth and 8.a passes and maximum stress amplitudes of approximately 85 MPa on the 7.a pass.

Stress time history of the individual local stress and stress spectra are obtained from numerical analysis and pass schedule. Fig. 11 shows the stress time history of the local stress on the 7th pass for only one billet.

5. Material

The material used for rolls was spheroidal graphite iron with a pearlitic base. The chemical composition of the roll material was 3.4–3.6% C, 1.8–2.2% Si, 0.5–1% Mn, < 0.05% P, <0.05% S, <0.5% Cr, 1.5–3% Ni and <0.2% Mo. The hardness on the roll surface was 380 HB. Fig. 12 shows the hardness drop of KGR 380 rolls and metallographic structure of the roll material.

The tensile strength of the core was 325–425 MPa and the bending strength of the core was 500–700 MPa. Because of unknown material fatigue strength data, the fatigue tests were carried out and fatigue life (service life) prediction was possible.

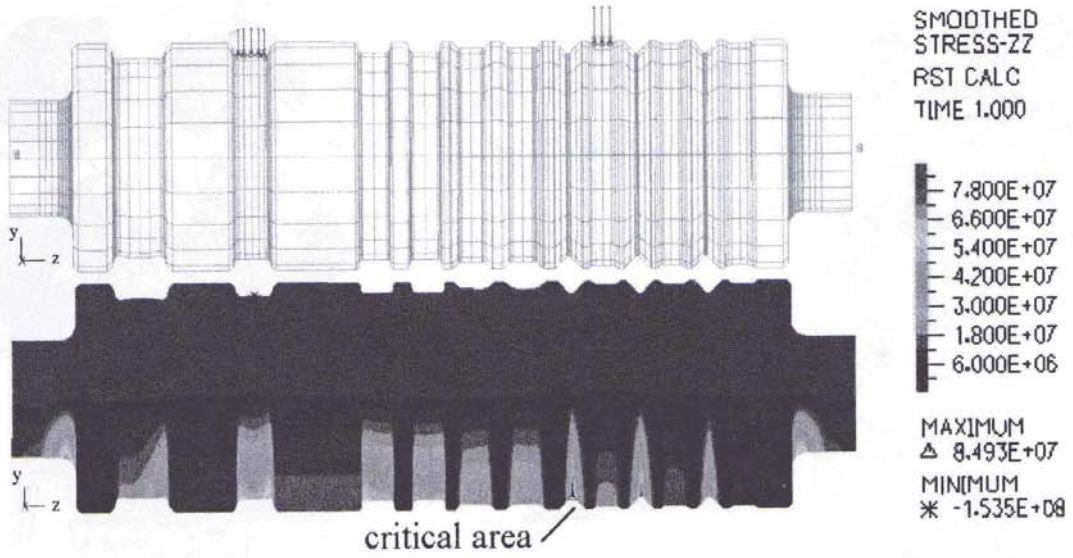

Fig. 10. Numerical (FEM) analysis.

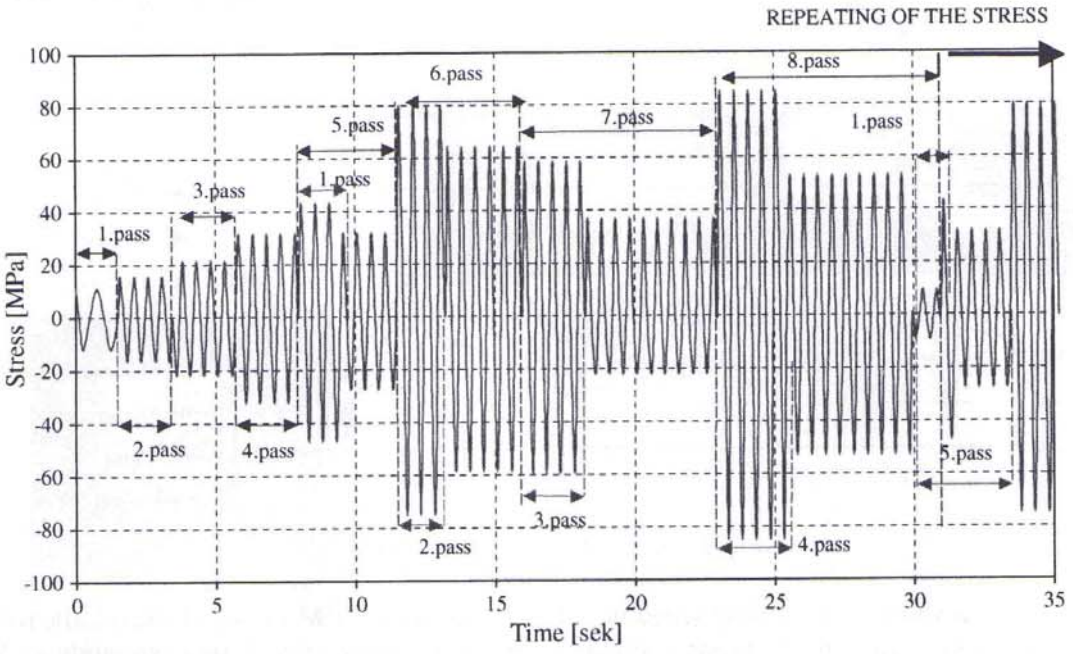

Fig. 11. Stress–time history at the critical area for one billet.

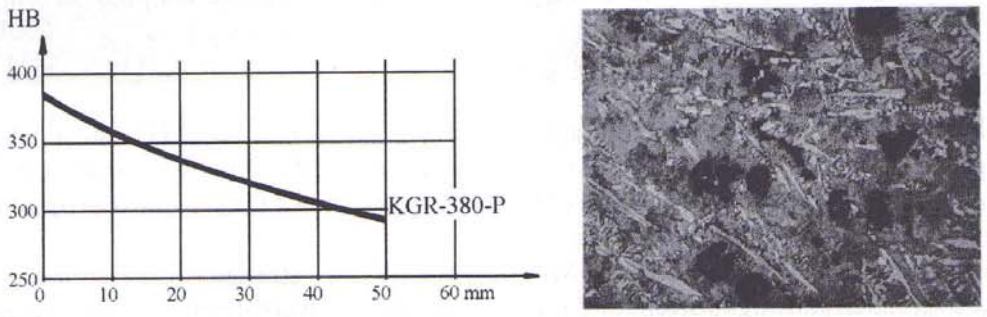

Fig. 12. Hardness drop and metallographic structure (500 ×).

Fig. 13 shows the fatigue strength of the roll material and stress spectra at the critical area for 4000 rolling tons.

From this diagram it can be seen that failures should be avoided in the normal service without overloads.

6. Overloads

The temperature of the rolling material has a great influence on the rolling forces. When the rolling process was carried out at a decreased temperature, the rolling forces are higher and bending stresses can be two or three times higher than is usually (Fig. 14).

During the rolling process some of the rolling stocks stayed on the rollers outside of the furnace due to the technological stops. The temperatures of these stocks were decreased due to the cooling by ambient air. No temperature sensors of rolling stock between the furnace and the 3-high-roughing mill stand were anticipated and there was no control of the decreasing rolling temperature between the furnace and the 3-high-roughing mill stand. Because of this fact the rolls were occasionally subjected to higher rolling forces and bending overloads as a result of the technological stops.

7. Safety parts

The rolls are protected from bending overload with the safety parts (Fig. 8). In the case of the bending overload, one (or both) safety part has to fail before the failure of the roll. The material used for safety parts is flake graphite iron GG20 according to DIN. Fig. 15 shows the safety parts design.

The analysis of safety parts design showed that the safety parts have to fail if the rolling temperature is 900 °C.

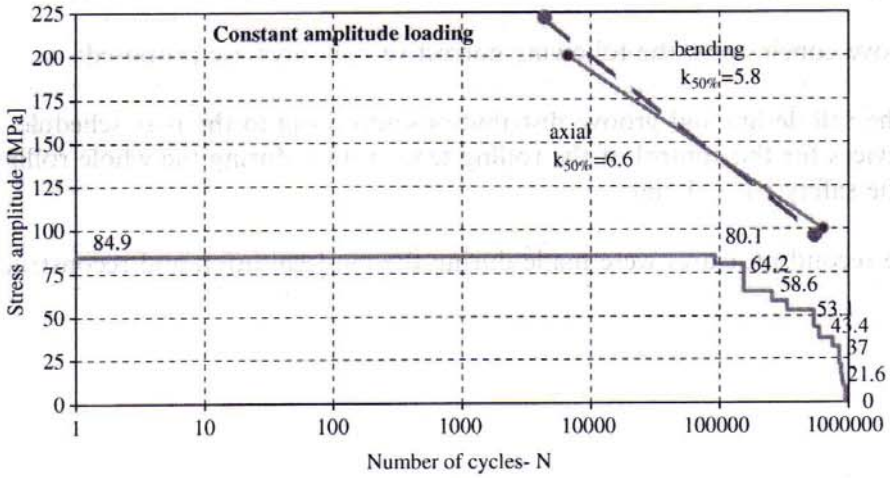

Fig. 13. Fatigue strength of the roll material and stress spectra at critical area for 4000 rolling tons.

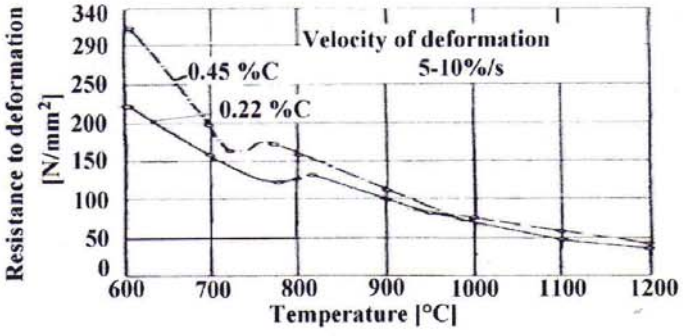

Fig. 14. Resistance to deformation of carbon steels related to temperature.

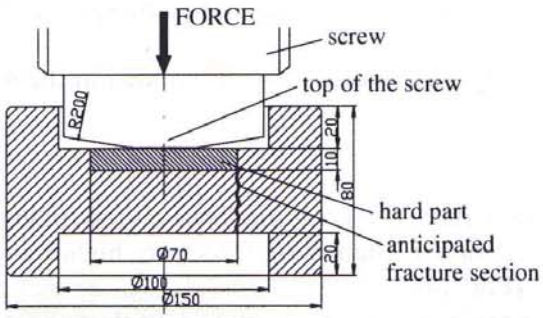

Fig. 15. Safety part.

In all cases of the roll failures, the failure of safety parts did not occur.

8. Concluding remarks

The following general conclusions are drawn out from the described failure analysis:

- Three out of four rolls fractured due to the low-cycle fatigue resulting from the rotational-bending loading with the high stress concentration. The fracture of the fourth roll occurred rapidly due to the bending overload by a dynamic impact.
- The bending overload was the consequence of the decreasing rolling temperature which has been caused due to the technological stops.
- Safety parts, designed to prevent failure of the rolls, did not perform their function.

Based on the above conclusions, the following corrective measures are proposed:

- The change of the roll design and groove distributions according to the pass schedule.
- To install the devices for the control of the rolling temperature during the whole rolling process.
- The change of the safety parts design.

The first and the second measures were made during the modernisation and reconstruction of the plant.